DINAME 2023 - Proceedings of the XIX International Symposium on Dynamic Problems of Mechanics,
A.S. De Paula, A.T. Fabro and M.R. Machado (Editors), ABCM.
Pirenópolis, Go, Brazil, February 26th to March 3rd, 2023

Identification of Unbalance and Shaft Bow in a Flexible Rotor Supported by Active Magnetic Bearings.

Gilberto Machado da Silva [1], Robson Pederiva [2]

[1] Herminio Ometto University Center and Technology College - Arthur Azevedo - Rua Ariovaldo Silveira Franco, 567 - Jd. 31 de Março - Mogi Mirim - SP – Brasil – Zip Code: 13801005 – gilberto.silva29@fatec.sp.gov.br

[2] University of Campinas – UNICAMP- Faculty of Mechanical Engineering - PO box 6122, Campinas – SP – Brasil, Zip Code: 13083970 - robson@fem.unicamp.br

Abstract: This paper presents a formulation for unbalance and shaft bow fault identification in flexible rotors supported by active magnetic bearings, AMB. The model-based procedure makes use of the correlation equations, through the matrix formulation of Lyapunov for linear systems along with artificial neural networks. This procedure only uses measured state variables from rotor position sensors and from the control states, measured in the time domain. Artificial neural networks are used to map correlations involving states that are not measured. Through the correlation of the output variables, a group of relations involving the physical parameters of the system together with the correlations of the measured variables is generated. By the difference between the measured correlations (with fault) and the expected correlations (without fault) was calculated. Through these differences and the neural network where the error manifests, the type of fault and its location in the system are concluded upon. Faults are identified considering various rotor unbalance configurations subjected to the shaft bow. A comparison of the theoretical and experimental results showed good agreement and the proposed procedure proved consistent in identifying two faults that can occur simultaneously in real cases.

INTRODUCTION

Modern Rotary machines have become increasingly complex and sophisticated. The development of materials, whether it is new alloys or composite materials, lighter and more resistant, allow to work at higher and higher rotations, supercritical rotations, high operating loads, and high reliability. Therefore, active magnetic bearings (AMBs) have progressively received importance compared with conventional bearings in many industrial applications. Are used in equipment in which the elimination of contact surfaces enables a very low mechanical wear, a decrease in motor consumption and the disposal of lubricants. They are suitable for the construction of sealed machines, which need to operate in a vacuum or in atmospheres subject to contamination (Prasad and Narayanan, 2021).

A rotating machine whether supported by magnetic bearing, or conventional bearings, may be subject to electrical faults such as control faults, sensor or actuators (Zhang et al., 2013) or subjected to mechanical faults, which are associated primarily with the rotor. Mechanical faults can occur during the assembly, service life, or maintenance; further, they include transverse cracks (Cavalini Jr et al., 2016), shaft bow (Sarmah and Tiwari, 2020), misalignments (Tuckmantel et al., 2019), bearing faults (Gunerkar et al., 2019), and unbalance faults. Several authors classify unbalance fault as the most common mechanical faults that can occur with a rotor followed by shaft bow and misalignment. Shaft bow can be developed due to the action of weight force on long horizontal rotors, due to thermal distortion, due to asymmetrical heating and cooling of the rotor, due to the unbalance force itself or due to friction of the rotor with some kind of seal (Mogal and Lalwani, 2017). Many studies have investigated the identification of rotor imbalances and other mechanical faults related to the rotor. Nicholas et al. (1976) makes the pioneer study the unbalance response of a rotor in the presence of the shaft bow. Rao (2001) studied the influence the bow on rotor response phase. Concluded that the response phase is more important than amplitude behavior when the bow is present. Darpe et al. (2006) carried out studies of the influence the residual bow effect on the stiffness variation of the cracked rotor through the analysis of the rotor in steady state and transient state. Song et al. (2013) used wavelets transform to identified experimentally residual shaft bow in a rotor/bearing system in the presence of noise. Sanches and Pederiva (2018) proposed a methodology based on correlation analysis and least squares fitting to generate an algorithm that can experimentally identify the unbalance and shaft bow in a rotor to overcame the practical difficulty in measuring certain responses by adopting a mathematical model reduced by the system equivalent reduction expansion process method (SEREP). Sarmah and Tiwari (2020) explored transverse crack and shaft bow in an AMB/rotor system excited by unbalance forces.

The problem of fault detection applied to rotational system with magnetic bearing has a special difficulty because the mechanical system equations are associated to the system control structure. The measurement of all state variables normally is not possible in real systems and the knowledge of stiffness and damping values are difficult to be identified. To avoid this practical characteristic, we propose a methodology that works with the structure of the model and generate compatibility equations involving correlations between a reduced numbers of state variables. These relations are obtained

by the matrix equation of Lyapunov. Eduardo and Pederiva, 2002 introduced this approach for fault detections. They developed a fault detection method based on the Lyapunov matrix equation that identifies the relationships between the physical parameters of the system using a set of correlation equations. Because it is not possible to measure all signals, they used ANNs to map the missing correlations. Sanches and Pederiva (2016) proposed a methodology based on correlation analysis and least-squares fitting to generate an algorithm that can experimentally identify the unbalance and shaft bow in a simple rotor. A more complex rotor was developed using the same methodology; however, Sanches and Pederiva (2018) overcame the practical difficulty in measuring some responses by adopting a mathematical model reduced by the system equivalent reduction expansion process method (SEREP). Silva and Pederiva (2006) applied correlation functions and ANNs for the detection of faults in a flexible rotor supported by AMBs with feedback control, and they detected sensor and actuator faults and shaft damages in a rotor. In another study, Silva and Pederiva (2018) theoretically explored rotor imbalance detection. Silva and Pederiva (2019) studied detection of electrical faults associated to control and sensors. Recently, Silva and Pederiva (2022) investigated experimentally; unbalance faults and electrical faults associated to the magnetic bearing and control system. Based on previous studies, this work proposes the identification of rotor unbalance associated with the shaft bow.

MATHEMATICAL APPROACH FOR DEVELOPING THE PROPOSED METHOD

The system under study consists of a rotor composed of flexible shaft on which are mounted four disks. In the external disks, there is a pair of active magnetic bearings, on the inner disks the motor and the rotation sensor, shown in Fig. 1.

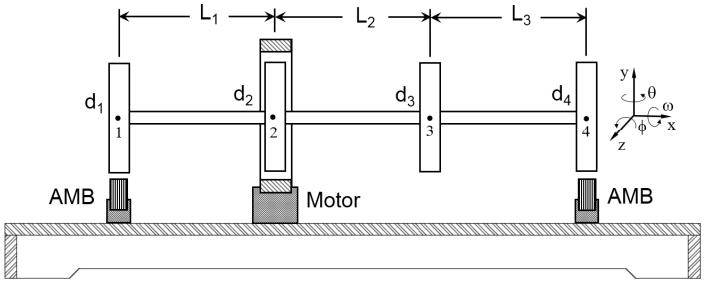

Figure 1 – System configuration.

The rotor model can be represented by the following differential equation:

$$\mathbf{M}\ddot{\mathbf{q}}(t) + \mathbf{G}\dot{\mathbf{q}}(t) + \mathbf{K}\mathbf{q}(t) = \boldsymbol{f}(t) \tag{1}$$

The equation of motion is composed of the generalized coordinate's vector $\boldsymbol{q}$(t) and its time derivatives. The vector $\boldsymbol{q}$(t) represents the displacements (y and z) and rotations (ϕ and θ) of the system, where

$$\mathbf{q}(\boldsymbol{t}) = [y_1 \;\; y_2 \;\; y_3 \;\; y_4 \;\; z_1 \;\; z_2 \;\; z_3 \;\; z_4 \;\; \phi_1 \;\; \phi_2 \;\; \phi_3 \;\; \phi_4 \;\; \theta_1 \;\; \theta_2 \;\; \theta_3 \;\; \theta_4]^{\boldsymbol{T}} \tag{2}$$

In Eq. (1), matrices **M**, **G**, and **K** denote the mass, gyroscope effect, and stiffness matrices, respectively. In addition, the force vector $\boldsymbol{f}(t)$ includes the magnetic force f_m(t), unbalance force f_u(t), and perturbation force h(t), which are the random white noise types. The vector **q**(t) represents the displacements (y and z) and rotations (ϕ and θ).

Unbalance force modeling

The unbalance force is proportional to the unbalance mass, its eccentricity, and the rotation of the rotor. Each disk is located in different radii of eccentricity and angular positions. Considering that the unbalance mass is smaller than the disk mass, the unbalance force can be expressed as

$$\begin{Bmatrix} f_y \\ f_z \end{Bmatrix} = \mathrm{m_u r_u}\, \omega^2 \begin{Bmatrix} \cos(\omega t + \beta) \\ \sin(\omega t + \beta) \end{Bmatrix} \tag{3}$$

where m_u, r_u, β, and ω denote the unbalance mass, unbalance radius, phase of unbalance, and spin speed of the rotor, respectively. The complete vector of the unbalance forces is given by

$$\boldsymbol{f}_{\mathrm{u}} = [f\mathrm{y}_1 \;\; f\mathrm{y}_2 \;\; f\mathrm{y}_3 \;\; f\,\mathrm{y}_4 \;\; f\mathrm{z}_1 \;\; f\mathrm{z}_2 \;\; f\mathrm{z}_3 \, f\mathrm{z}_4]^T \tag{4}$$

Shaft bow modeling

Assuming that the rotor system is balanced, a shaft bow causes an offset of the discs mass center δ in relation to the line passing through the center of the bearings. The shaft bow is modeled as an elastic restoring force acting on the equilibrium position (Sanches and Pederiva, 2018). As shown in Fig. 2.

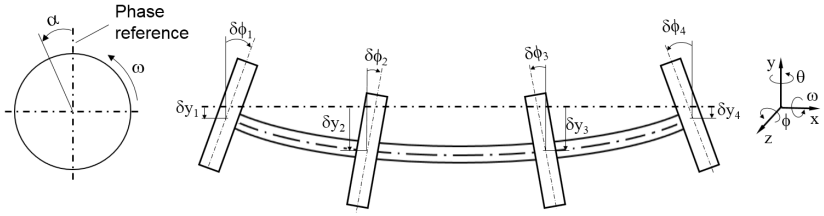

Figure 2 – Schematic view of a bowed shaft.

In Fig. 2 δy_i represents the linear bow, $\delta\phi_i$ is the angular bow caused by shaft arching, and α_i is the shaft bow phase. The bow force is a constant quantity synchronous with rotation, by Hooke's law is given by

$$\boldsymbol{f}_e = \mathbf{K}\,\boldsymbol{\delta}_\mathbf{i} \tag{5}$$

In Eq. (5) $\boldsymbol{f}_e$ represents the shaft bow force, $\mathbf{K}$ is the shaft stiffness matrix, $\boldsymbol{\delta}_i$ is the residual shaft bow vector, and i represents the node where bending occurs (i=1, 4).

Mechanical model in the form of state space

The mechanical system is represented in the state-space form as

$$\dot{\mathbf{x}}_m(t) = \mathbf{A}_m\mathbf{x}_m(t) + \mathbf{B}_m(t)\,\boldsymbol{f}(t) \tag{6}$$

$$\mathbf{z}_m(t) = \mathbf{C}_m\mathbf{x}_m(t) \tag{7}$$

In Eqs. (6) and (7), $\mathbf{A}_m$, $\mathbf{B}_m$, and $\mathbf{C}_m$ are dynamic, input, and output matrices, respectively; $\mathbf{z}_m$ denotes the vector of the measured mechanical states; $\mathbf{x}_m(t)$ represents the mechanical state vector; and the dots indicate time derivatives.

AMB and Controller Model

The configuration of a magnetic bearing is shown in Fig. 3. The magnetic force is inversely proportional to the distance, and when applying and magnetic force to the rotor the tendency is to be attracted to the minimum possible distance between its surface and the electromagnet. In closed loop, the system operates by reading the sensor that determines the position of the rotor. In this case, as the sensor is not positioned in the direction of actuation, the sensor reading is added through an equivalent gain that passes to the controllers reading of the displacements of each direction (y and z). The controller process the information and send to the power amplifier a signal that is converted in a proportional signal of current. This signal is sent to the bearing actuator coil and trans-formed into magnetic force through the actuator gains, working in closed loop.

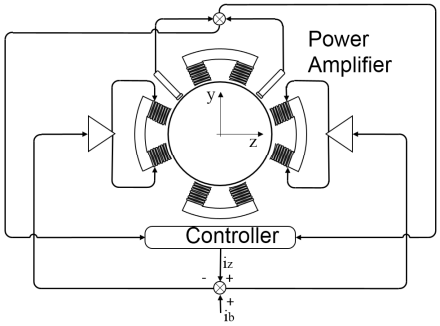

Figure 3 - Schematic representation of a radial AMB.

The force applied to the rotor in a pair of coils can be expressed by the following expression for the two half-axes (Schweitzer and Maslen, 2009)

$$f_m = k_i i_c - k_z z \tag{8}$$

$$k_i = \frac{4\,k_m\,i_b}{g^2} \tag{9}$$

$$k_z = \frac{4\,k_m\,i_b^2}{g^3} \tag{10}$$

$$k_m = 0.25\,\mu_0\,N^2\,A_0 \tag{11}$$

where k_z denotes the displacement stiffness of the bearing; it is directly incorporated into the mechanical stiffness matrix and is the so called negative spring; k_i denotes the current stiffness of the bearing, i_b denotes the bias current; g denotes the air gap; μ_0 denotes the permeability of free space; N denotes the number of windings; A_0 denotes the cross-sectional area of flux in the air that is equal to the area of the iron core; and km represents the gain of the magnetic actuator.

A sixth-order analog control was used to satisfy the dynamic characteristics of the system. For each axis of action, there is an independent controller called the single in single out (SISO) controller. The model of control in the form of the state space is given as

$$\dot{\mathbf{x}}_c(t) = \mathbf{A}_c\mathbf{x}_c(t) + \mathbf{B}_c(t)\,\mathbf{u}(t) \tag{12}$$

$$\boldsymbol{f}_m = \bar{\mathbf{C}}_c\,\mathbf{x}_c(t) \tag{13}$$

$$\mathbf{u}(t) = k_s\,\mathbf{z}_m \tag{14}$$

$$\bar{\mathbf{C}}_c(t) = \mathbf{C}_c\,k_m\,k_p \tag{15}$$

where $\mathbf{A}_c$, $\mathbf{B}_c$, and $\bar{\mathbf{C}}_c$ denote the dynamic, input, and output matrices of the control, respectively, $\mathbf{x}_c$ denotes the vector of the control states plus the k_m and k_p gains of the magnetic actuator and power stage, respectively; and $\mathbf{u}(t)$ denotes the input tension arising from the rotor displacements with the sensor gain. For each actuation direction, there are six states of control.

The final equation in the state space composed by the mechanical and control models given by

$$\dot{\mathbf{x}}_f(t) = \mathbf{A}_f\mathbf{x}_f(t) + \mathbf{B}_f\boldsymbol{f}(t) \tag{16}$$

where

$$\mathbf{A}_f = \begin{bmatrix} \mathbf{A}_m & \mathbf{B}_m\mathbf{C}_c \\ \mathbf{B}_m\mathbf{C}_c & \mathbf{A}_c \end{bmatrix},\ \mathbf{B}_f = \begin{bmatrix} \mathbf{B}_m \\ \mathbf{Z} \end{bmatrix} \text{ and } \mathbf{x}_f = \begin{bmatrix} \mathbf{x}_m \\ \mathbf{x}_c \end{bmatrix} \tag{17}$$

In Eq. (17) $\mathbf{A}_f$ and $\mathbf{B}_f$ are the dynamic and input matrices of the complete system, respectively; $\boldsymbol{f}(t)$ denotes the external excitation vector composed of unbalance forces, magnetic forces, and white noise perturbation; $\mathbf{x}_f$ denotes the vector in the state space with the system in the closed loop; and $\mathbf{Z}$ represents the zero matrix.

The invariant system with stationary inputs is considered. Under these conditions, the correlation functions assume values constant in time and depend only on the time interval (Eduardo and Pederiva, 2002)

$$\mathbf{R}x_f(\tau_i) = \varepsilon\{\mathbf{x}_f(t).\,\mathbf{x}_f{}^T(t+\tau_i)\} \tag{18}$$

where ε denotes the mathematical expectation, and τ_i denotes the time interval.

Replacing the solution of Eq. (16) in Eq. (18), we have:

$$\mathbf{A}_f\,\mathbf{R}x_f + \mathbf{R}x_f\,\mathbf{A}_f^T + \mathbf{B}_f\,\mathbf{R}x_e x_f + \mathbf{R}x_f x_u\,\mathbf{B}_f^T = 0 \tag{19}$$

Equation (19) represents the Lyapunov matrix equation for stationary linear systems, and it is possible to establish a relationship between the physical parameters of the system and the correlation functions, which is the basis of the proposed diagnostic method.

$$\mathbf{R}x_f = \begin{bmatrix} \mathbf{R}x_m x_m & \mathbf{R}x_m x_c \\ \mathbf{R}x_c x_m & \mathbf{R}x_c x_c \end{bmatrix},\ \mathbf{R}\,x_e x_f = [\mathbf{R}x_e x_m \quad \mathbf{R}x_e x_c] \text{ and } \mathbf{R}x_f x_e = \begin{bmatrix} \mathbf{R}x_m x_e \\ \mathbf{R}x_c x_e \end{bmatrix} \tag{20}$$

In Eq. (20): $\mathbf{R}x_m x_m$ is the matrix of correlations between the mechanical states, $\mathbf{R}x_m x_c$ is the matrix of correlations between the mechanical states and states of control , $\mathbf{R}x_c x_m$ is the matrix of correlations between the states of control and mechanical states, $\mathbf{R}x_c x_c$ is the matrix of correlations between the states of control, $\mathbf{R}x_e x_m$ is the matrix of correlations between the excitation and mechanical states, $\mathbf{R}x_e x_c$ is the matrix of correlations between excitations and states of control, $\mathbf{R}x_m x_e$ is the matrix of correlations between the mechanical states and excitations and $\mathbf{R}x_c x_e$ is the matrix of correlations between the states of control and excitations.

The development of Eq. (19) results in a matrix where each term corresponds to a correlation equation, and the equations selected according to the system parameters associated with each equation for developing the method are presented below.

The equation associated with the mechanical state z_1 is:

$$k_{13,5}Rz_1z_1 + k_{13,6}Rz_1z_2 + k_{13,13}Rz_1\theta_1 + k_{13,14}Rz_1\theta_2 + g_{13,5}Rz_1\dot{z}_1 + g_{14,5}Rz_1\dot{z}_2 + g_{13,5}Rz_1\dot{\phi}_1 + g_{13,10}Rz_1\dot{\phi}_2 + b_{5,21}Rz_{e1}z_1 = 0 \quad (21)$$

The equation associated with the mechanical state z_2 is:

$$k_{14,5}Rz_2z_1 + k_{14,6}Rz_2z_2 + k_{14,7}Rz_2z_3 + k_{14,13}Rz_2\theta_1 + k_{14,15}Rz_2\theta_2 + k_{14,16}Rz_2\theta_3 + g_{14,5}Rz_2\dot{z}_1 + g_{14,6}Rz_2\dot{z}_2 + g_{14,7}Rz_1\dot{z}_3 + g_{14,9}Rz_2\dot{\phi}_1 + g_{14,10}Rz_2\dot{\phi}_2 + g_{14,11}Rz_2\dot{\phi}_3 + b_{6,22}Rze_2z_2 = 0 \quad (22)$$

The equation associated with the mechanical state z_3 is:

$$k_{15,6}Rz_3z_2 + k_{15,7}Rz_3z_3 + k_{15,8}Rz_3z_4 + k_{15,14}Rz_3\theta_2 + k_{15,15}Rz_3\theta_3 + k_{15,16}Rz_3\theta_4 + g_{15,6}Rz_3\dot{z}_2 + g_{15,7}Rz_3\dot{z}_3 + g_{15,8}Rz_3\dot{z}_4 + g_{15,10}Rz_2\dot{\phi}_2 + g_{15,11}Rz_3\dot{\phi}_3 + g_{15,12}Rz_3\dot{\phi}_4 + b_{7,23}Rz_{e3}z_3 = 0 \quad (23)$$

The equation associated with the mechanical state z_4 is:

$$k_{16,7}Rz_4z_3 + k_{16,8}Rz_4z_4 + k_{16,15}Rz_4\theta_3 + k_{16,16}Rz_4\theta_4 + g_{16,7}Rz_4\dot{z}_3 + g_{16,8}Rz_4\dot{z}_4 + g_{16,11}Rz_4\dot{\phi}_3 + g_{16,12}Rz_4\dot{\phi}_4 + b_{8,24}Rz_{e4}z_4 = 0 \quad (24)$$

Initially, the displacements and speeds in the four rotor discs, in addition to the five control states in the same direction, are considered as the states that can be measured. It is interesting to note among the selected correlation equations, there are different relationships with the physical parameters of the system. Any change in given parameter that is related to the equation will cause changes in the equality of the respective equation. This change is an indication that the equation is sensitive to the change of this parameter. The unbalance and bowing force are related to the mechanical input matrix $\mathbf{B}_m$, Eq. (6). In Eqs. (21) – (24), there are relationships with the stiffness of the shaft elements k_{ij}, related to the parameters of the gyroscopic matrix terms g_{ij}, and parameters b_{ij} are terms of the input matrix of the mechanical system, and they are related to the excitation forces: the unbalance force and noise. The autocorrelation $\mathbf{R}z_1z_1$ was isolated from the right side of Eq. (20), $\mathbf{R}z_2z_2$ from Eq. (21), $\mathbf{R}z_3z_3$ from Eq. (22) and $\mathbf{R}z_4z_4$ from Eq. (23). In all cases, the other parameters were divided by the parameter related to each isolated auto correlation. Terms difficult to measure were excluded and possible measurement correlations were entered as neural network inputs. The terms isolated at the output of each neural network corresponding to each selected compatibility equation, are shown in Tab. 1.

Table 1 – Inputs and output of ANNs.

disc	est.	inputs	output	ANN
d_1	z_1	$\mathbf{R}z_1z_2, \mathbf{R}z_1\dot{z}_1, \mathbf{R}z_1\dot{z}_2, \mathbf{R}z_{e1}z_1$	$-\mathbf{R}z_1z_1$	A_1
d_2	z_2	$\mathbf{R}z_2z_1, \mathbf{R}z_2z_3, \mathbf{R}z_2\dot{z}_1, \mathbf{R}z_2\dot{z}_2, Rz_1\dot{z}_3, \mathbf{R}z_{e2}z_2$	$-\mathbf{R}z_2z_2$	A_2
d_3	z_3	$\mathbf{R}z_3z_2, \mathbf{R}z_3z_4, \mathbf{R}z_3\dot{z}_2, \mathbf{R}z_3\dot{z}_3, \mathbf{R}z_3\dot{z}_4, \mathbf{R}z_{e3}z_3$	$-\mathbf{R}z_3z_3$	A_3
d_4	z_4	$\mathbf{R}z_4z_3, \mathbf{R}z_4\dot{z}_3, \mathbf{R}z_4\dot{z}_4, \mathbf{R}z_{e4}z_4$	$-\mathbf{R}z_4z_4$	A_4

Figure 4 illustrates the structure of neural networks A_1 that will be used for monitoring and diagnosing defects in the AMB/rotor system. Architectures A_1, A_2, A_3, and A_4, were trained with a system without fault and without noise. The neural networks used have 1 input layer, 1 intermediate layer with 10 neurons each, using a sigmoidal activation function and an output. For the training of the networks the Levenberq - Marquart algorithm was used. By the difference between the output correlations (with fault) and the expected correlations (without fault) was calculated. Through these differences and the neural network where the error manifests, the location in the system are concluded upon.

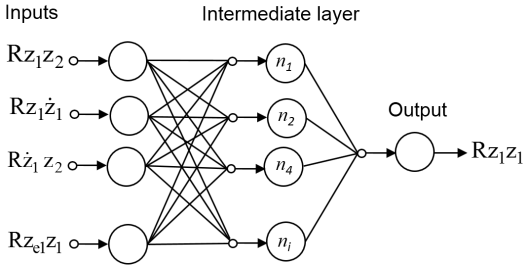

Figure 4 - Structure of ANN A_1.

The mean square deviation (MSD) is used as an indicator of the presence of faults in the system (Eduardo and Pederiva, 2002).

$$\mathrm{MSD} = \left(\frac{1}{\mathrm{N}}\sum_{\mathrm{i}=1}^{\mathrm{N}}(\mathbf{R}\,\mathrm{x}_f - \overline{\mathbf{R}}\mathrm{x}_f)^2\right)^{1/2} \tag{25}$$

where $R\mathrm{x}_f$ and $\overline{R}\mathrm{x}_f$ denote the output (system with fault) and expected output autocorrelations (without fault), respectively, and N denotes the number of training data.

NUMERICAL AND EXPERIMENTAL RESULTS

The time domain response of the system was obtained through MatLab - Simulink software. The Simulink model is essentially made of a block consisting of space of mechanical states equations, Eq. (9), whose output are the displacements y_1, z_1, y_4 and z_4 that pass through the gains of the sensors and feed the four blocks composed by the equations of Eq. (8); their outputs pass through the bearing gains and power stage that feedback with the magnetic force in each direction of actuation of the magnetic bearing. The system is excited by external unbalance force and white noise. The mechanical states y_1, y_2, y_3, y_4, z_1 z_2, z_3 and z_4 are obtained simultaneously and the six control states in the direction Z1c and in the direction Z4c in fixed rotation of 3000 RPM. The fault-free system parameters are listed in Tab. 2.

Table 2 – Physical properties of the rotor and AMBs.

Discs	Parameter	Value	Unit
Mass	m_d	$8.80\ 10^{-2}$	kg
Moment inertia	I_d	$3.10\ 10^{-5}$	$kg.m^2$
Polar moment of inertia	I_p	$6.02\ 10^{-5}$	$Kg.m^2$
Shaft	**Parameter**	**Value**	**Unit**
Length	L_1,L_2,L_3	0.150	m
Cross section	A_{shaft}	$1.57\ 10^{-5}$	m^2
Moment of inertia of area	I_e	$5.10\ 10^{-11}$	m^4
AMB's	**Parameter**	**Value**	**Unit**
Gain of the sensor	k_s	1900	V/m
Gain of the power amplifier	k_p	-0.25	A/V
Gain of the bearing	k_m	8	N/A
Negative spring	k_z	-2450	N/m
Bias current	i_b	0.307	A
Air gap	g	10^{-3}	m

The artificial neural networks were implemented in the MATLAB software. The Levenberg–Marquardt backpropagation is the selected training function. This training function updates the weight and bias values according to the Levenberg–Marquardt optimization. In the simulation, the default weight settings of the software were used. However, during training, it is possible to monitor the synaptic weights. The different order of magnitude in the synaptic weights is a symptom of network instability.

Under the operating conditions, every rotating machine was subjected to noise to test the skill of the ANN to map the missing correlations in the presence of colored noise; several magnitudes of random noise were summed to the excitation. The levels of colored noise were tested; the magnitude of noise added to the system was measured based on the RMS value of the magnitude of unbalance force. The values of the output correlations were considered with and without noise, and the comparison was conducted using the mean square error MSD given by Eq. (25). As shown in Tab. 3.

Table 3 – MSD: Magnitudes of colored noise added to the excitation.

	MSD [%]			
Noise level	A_1	A_2	A_3	A_4
5%	0.311	0.260	0.106	0.492
10%	0.657	1.712	0.493	0.423
15%	1.547	1.900	1.058	1.549

From the results presented in Tab. 3, it is noted that the neural networks proved to be robust and maintained their mapping capacity in the presence of colored noise; the values are negligible when compared to the failed system. The values show that the method does not take the presence of noise as a possible fault.

The test bench, shows in Fig. 5, designed for the experimental analysis comprises a flexible hollow aluminum shaft mounted on four discs constructed in two parts and an aluminum core mounted with an outer ring. The discs where the coils of the magnetic bearing operate received a ring comprising a packet of silicon iron sheets, which possess good magnetic characteristics. The discs where the motor and the rotation sensor operate received a steel ring. The induction motor comprised a set of three-phase coils in the stator, thereby creating a rotating field that acts on an iron magnetic metal ring, called a hysteresis ring. The displacement sensors are eddy-current magnetic sensors, and they were mounted at 45º from the *Y* and *Z* axes, close to discs d_1 and d_4 because of the size of the head of the magnetic bearing coils. The actuators are composed of a pair of coils in each direction with a ferromagnetic material core to avoid losses. The circuit is closed through the ferromagnetic laminated material of the rotor, and it is dimensioned considering the required load capacity, dimensional, thermal, and magnetic saturation limitations.

Before assembling the rotor on the workbench, impact tests were conducted with the rotor suspended through a bump test. With the aid of a dynamic signal analyzer (HP35677A, Hewlett Packard), the rotor was excited with a hammer with a load cell. The displacement was measured using an accelerometer fixed in the same direction.

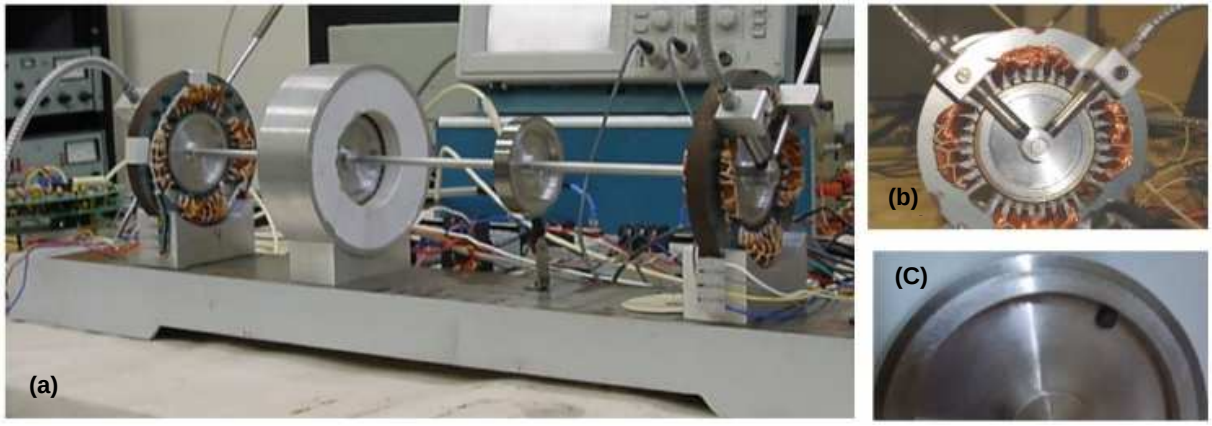

Figure 5 - Experimental test rig. (a) Rotor, motor, rotation sensor, and AMBs. (b) Close view of disk and sensors. (c) Close view of mass imbalance.

The first three mode shape frequencies were measured and compared with the values obtained by the model shows in Tab. 4.

Table 4 – Natural frequencies of the rotor without AMBs.

	First mode shape (Hz)	Second mode shape (Hz)	Third mode shape (Hz)
Simulated	22,3	72,6	204,7
Experimental	23,0	73,0	206,0

After, the rotor was alignment and was measurement of the position of the discs. The external disks were supported on a V-block and with the dial gauge; the alignment of the disks was performed. The residual bow shows in Tab. 5.

Table 5 – Residual shaft bow

disc	d_1	d_2	d_3	d_4
Mag. [μm] / phase [graus]	0 μm / 0º 0 μm / 90º	15 μm / 0º 10 μm / 90º	10 μm / 0º 8 μm / 90º	0 μm / 0º 0 μm / 90º

After assembling, the rotor was balanced by the coefficient of the influence method. Four planes, disks (d_1, d_2, d_3, and d_4), and the readings obtained using the sensors of disks d_1 and d_4 were used for the balancing. A portion of beeswax glued to the disk, Fig. 5(c) was used as the unbalance mass. Balancing was performed with two rotations at 1200 rpm and at a nominal rotation of 3000 rpm, where the residual unbalance masses and their phases were estimated; this operating condition was considered for the system without fault in the experiment. As shown in Tab. 6.

Table 6 – Residual unbalance

disc	d_1	d_2	d_3	d_4
Mass [g] / phase [graus]	0,02 g / 30º	0,05 g / 90º	0,08 g / 180º	0,04 g / 0º

Experimentally the time domain response of the system was obtained from text bench. Figure 6 shows the positioning of measured states. The data were conditioned on an acquisition board that converts the analog signal to a digital signal for signal processing. The NI USB-6251 model (National Instruments) was used as the card. The board has 16 analog inputs with 16 bits of resolution plus 2 analog outputs and 2 digital inputs and outputs; it operates at a maximum sampling frequency of 1.25 MS/s. Sampling times of 20 s and a sampling frequency of 2500 Hz were used.

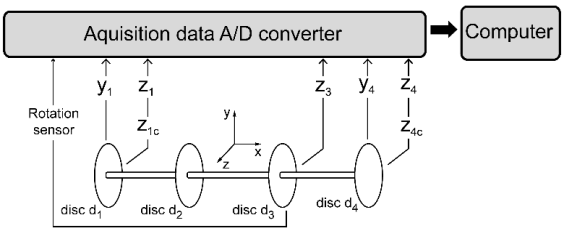

Figure 6 - Positioning of measured states.

Figure 7 compares the experimental and simulated displacement rotor, state control, and correlations of the system fully levitated on the AMB at 3000 rpm, only residual shaft bow and unbalance.

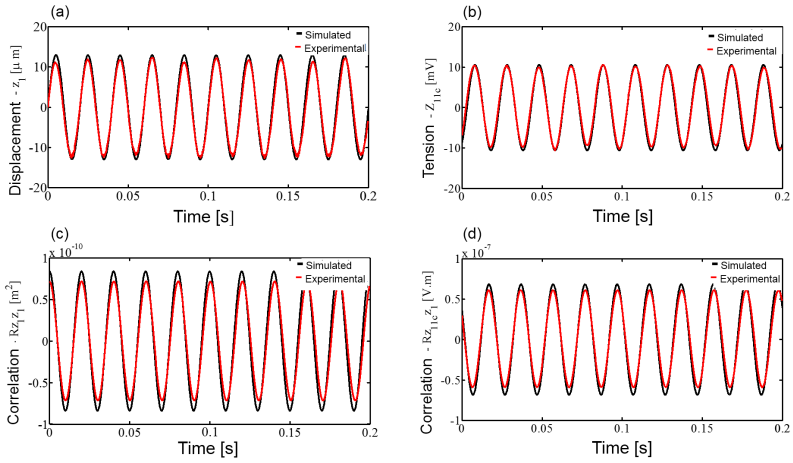

Figure 7. (a) Displacement rotor z_1. (b) State control z_{11c}. (c) Correlation Rz_1z_1. (d) Correlation RZ_{11c} Z_1.

Figure 8 (a) shows the numerical shaft bow response of (15 and 10 μm at 0°) associated with the respective bow angles on all discs and residual unbalance (0.1 g at 0°) on all discs respectively. Figure 8 (b) shows the theoretical and experimental shaft and unbalance responses.

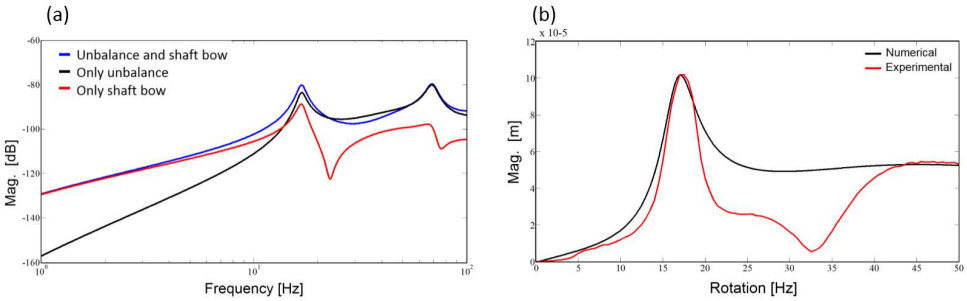

Figure 8 - (a) Comparison - Unbalance response and shaft bow response and (b) Comparison Numerical and experimental unbalance and shaft bow responses.

Sanches and Pederiva (2016) emphasize the difference between shaft bow response and unbalance response is in the difference in vibration amplitudes that occurs at low and high frequencies. The unbalance is predominant at high frequencies and in the case of shaft bow is predominant at low frequencies, as shown in Fig. 8 (a). Experimentally, the rotor is placed at the nominal speed of 50 Hz, the motor action is removed and the rotor is decelerated, with the aid of the

spectrum analyzer, the responses are obtained. The responses, whether in terms of frequency or amplitude, are coherent, as shown in Fig. 8 (b).

For 4 cases of simulated unbalance faults, all masses were always positioned within a radius of 25 mm. The values and phases of the unbalance masses and bow are summarized in Tab. 7. In all cases, the MSD error in Eq. (25) was calculated. The networks were trained with the residual masses and without noise. In the 4 cases of mass change, 10% of colored noise was added to the excitation.

Table 7 – Numerical results - Fault unbalance and shaft bowl configuration.

	Unbalance mass [g] / phase [degree] Shaft bow [μm] / phase [degree]				MSD [%]			
Case	disc - d_1	disc - d_2	disc - d_3	disc - d_4	A_1	A_2	A_3	A_4
Training	0.02g / 30º 0	0.05g / 90º 25μ m /180º	0.08g / 180º 20μ m /180º	0.04g / 0º 0	-	-	-	-
case#1	1.0g / 0º -	1.0g / 0º -	1.0g / 0º -	1.0g / 0º -	32.6	43.6	38.9	37.2
case#2	- 0	- 25μ m /180º	- 20μ m /180º	- 0	6.7	12.8	17.5	5.9
case#3	1.0g / 0º 0	1.0g / 0º 25μ m /180º	1.0g / 0º 20μ m /180º	1.0g / 0º 0	21.5	13.2	14.7	27.6
case#4	1.0g / 180º 0	1.0g / 180º 25μ m /180º	1.0g / 180º 20μ m /180º	1.0g / 180º 0	46.9	35.9	41.6	41.7

Table 7 indicates that by the neural network architectures presented is possible to detect fault to rotor unbalance and shaft bow. In case #1, in which the unbalance was imposed on all disks, the MSD values of all disks were significantly changed. In case #2, when bow was imposed only on the central disks, the highest MSD values occurred in the neural networks related to these disks. In case #3 the unbalance is in counter-phase with the bow, then there is a decrease in the MSD value which can be called a self-balancing because unbalance forces and bow forces were in opposite phases and in case #5 the opposite occurs bow and unbalance are in phase which increases the MSD value at the output of neural networks. In the experiment, the system was considered without fault with the configuration of residual unbalance masses and shaft bow. Further, it is important to emphasize that masses placed when the fault was imposed naturally were added to the residual masses. With the bench at the nominal rotation of 3000 rpm, all possible states of the measurement were acquired, because there was no sensor on disc d_2, and this measurement was impaired in the test. Compromising the inputs the neural networks A_1 e and A_2. As shown in Tab. 8.

Table 8 – Experimental results - Fault unbalance and shaft bowl configuration.

	Unbalance mass [g] / phase [degree] Shaft bow [μm] / phase [degree]				MSD [%]			
Case	disc - d_1	disc - d_2	disc - d_3	disc - d_4	A_1	A_2	A_3	A_4
Training	0.02g / 30º 0	0.05g / 90º 25μ m /180º	0.08g / 180º 20μ m /180º	0.04g / 0º 0	-	-	-	-
case#6	1.0g / 0º -	1.0g / 0º -	1.0g / 0º -	1.0g / 0º -	-	-	17.5	28.7
case#7	1.0g / 180º -	1.0g / 180º -	1.0g / 180º -	1.0g / 180º -	-	-	45.8	42.6

Considering the results shown in Tab. 8, the unbalance values identified it is similar to case #3 and 4, presented in Tab. 7. Although the network was trained with residual unbalance and bow, networks A_3 and A_4 detected the change in unbalance with bow effect (case #5 and 6). In case #6 the unbalance is in counter-phase with the bow, so there is a decrease in the MSD value, which can be called a self-balancing because unbalanced forces and bow forces are in opposite phases. In case #7 the opposite occurs, bow and unbalance are in phase, which increases the MSD value at the output of the neural networks, the bow increases the effect of the imbalance.

CONCLUSIONS

In this work, the fault detection method based on Ljapunov matrix equation and artificial neural networks in a flexible rotor with active magnetic bearings was presented. Through the method, it was possible to identify shaft bow and unbalance faults. For application of the proposed method, it is not necessary to know whether the values of the parameters of the model are electric or mechanical, only its structure in the model. Considering that several states are not possible to be measured, they are mapped by the neural networks. The method is insensitive to the addition of noise at the entrance, not taking this factor as possible fault. The experimental results were in agreement with the simulated results, and the difference between the two cases was not constant. Taking the mean absolute error between the four theoretical and

experimental results ranged from 2% to approximately 12%. These differences results because of possible differences between the model and the bench. In the model, it is assumed that the measurements take place in the center of the bearing, which is not possible to be done in the experiment. Sensors and actuators theoretically have equal gains in both directions (vertical and horizontal) which may not happen on the bench. In the experimental procedure, neural network A_1 and A_2 was excluded owing to the lack of measurement of displacement on disk d_2. For all other cases, the method proved efficient in the detection of failure due to balancing. In planes where the fault was to be detected, at least one displacement sensor in the plane was required. Despite this need, the use of the proposed method was found to be feasible in real cases, considering the good consistency of the numerical results with the experimental results and the robustness of the method.

ACKNOWLEDGMENTS

The authors would like to thank the Brazilian Navy Technology Center in São Paulo (CTMSP) for collaboration in the experimental part of this work.

REFERENCES

Prasad, K. N. V. and Narayanan, G., 2021, "Electromagnetic bearings with power electronic control for high - speed rotating machines: review, analysis, and design example", IEEE Transactions on Industry Applications, v. 57, pp. 4946 – 4947.

Zhang, Y. Z., Zhang L. Z., Luo, X. Y. and Guan, X. P., 2013, "Sensor/Actuator Faults Detection for Networked Control Systems via Predictive Control", International Journal of Automation and Computing, Vol. 10 (3), pp. 173 - 180.

Cavalini Jr., A.A., Sanches L., Bachschmid N. and Steffen Jr., V., 2016, "Crack identification for rotating machines based on a nonlinear approach", Mechanical Systems and Signal Processing, Vol. 79, pp. 72-85.

Sarmah, N. and Tiwari, R., 2020, "Analysis and identification of the additive and multiplicative fault parameters in a cracked-bowed-unbalanced rotor system integrated with an auxiliary active magnetic bearing", Mechanism and Machine Theory Vol. 146, pp. 1-25.

Tuckmantel, F. W. S and Cavalca, K. L., 2019, "Vibration signatures of a rotor-coupling-bearing system under angular misalignment", Mechanism and Machine Theory, Vol. 133, pp. 559-583.

Gunerkar, R. S, Jalan, A. K. and Belgamwar S. U., 2019, "Fault diagnosis of rolling element bearing based on artificial neural network", Journal of Mechanical Science and Technology, Vol. 33, pp. 505-511.

Mogal S.P. and Lalwani D.I., 2014, "A brief review on fault diagnosis of rotating machineries". Applied Mechanics and Materials Vol. 541–542, pp. 635–40.

Nicholas, J. C., Gunter, E. J. and Allaire, P. E., 1976 "Effect of residual shaft bow on unbalance response and balancing of a single mass flexible rotor Part I- Unbalance Response", Journal of Engineering for Power, Vol. 98, pp. 171-181.

Rao, J. S., 2001, "A Note on Jeffcott Warped Rotor", Mechanism and Machine Theory, Vol.36, pp. 563-575.

Darpe, A. K., Gupta K. and Chawla, A., 2006, "Dynamics of a bowed rotor with a Transverse surface crack", Journal of Sound and Vibration, Vol. 296, pp. 888-907.

Song, G. F., JI, C., Yang, Z. J. and Wang, F. P., 2013, 'Theoretical - experimental study on a rotor with a residual shaft bow', Mechanism and Machine Theory, Vol. 63, pp. 50-58.

Sanches, F. D. and Pederiva, R., 2018, "Simultaneous identification of unbalance and shaft bow in a two - disk rotor based on correlation analysis and the SEREP model order reduction method", Journal of Sound and Vibration, Vol. 433, pp. 230-247.

Eduardo A.C. and Pederiva R., 2002, "Parameter monitoring of a rotor system excited by stochastic forces", Proceedings of the 6th International Conference on Rotor Dynamics, Sidney, Australia, pp. 310–7.

Sanches F. D. and Pederiva R., 2016, "Theoretical and experimental identification of the simultaneous occurrence of unbalance and shaft bow in a Laval rotor", Mechanism and Machine Theory; Vol. 101, pp. 209–21.

Silva G.M. and Pederiva R., 2006, "Diagnosis in a rotor supported by active magnetic bearings", Proceedings of the International Conference on Rotor Dynamics, Vienna, Austria, pp. 25–8.

Silva G.M. and Pederiva R., 2019, "Unbalance Identification in a Rotor Supported by Active Magnetic Bearing", Proceedings of the 7th International Conference on Rotor Dynamics, Rio de Janeiro, Brazil, Vol 60, pp. 82-96.

Silva, G.M. and Pederiva, R., 2019, "Electrical fault detection in a rotor supported by active magnetic bearing". Proceedings of the XV International Symposium on Dynamic Problems of Mechanics, Búzios, Brazil, pp. 36 – 42.

Silva, G. M. and Pederiva, R., 2022, "Fault diagnosis of active magnetic bearings", Mechatronics, Vol. 84, pp. 1–15.

Schweitzer G. and Malsen E.H., 2009. "Magnetic bearings: Theory, design and application to rotating machinery". Berlin: Springer Verlag.

RESPONSIBILITY NOTICE

The authors are the only responsible for the printed material included in this paper.